Canted antiferromagnetism and excitonic order in gated double-layer graphene

V. Apinyan* and T. K. Kopeć

Institute of Low Temperature and Structure Research, Polish Academy of Sciences, P.O. Box 1410, 50-950 Wrocław 2, Poland

(Received 1 June 2023; revised 20 July 2023; accepted 4 August 2023; published 21 August 2023)

We study the effects of electron-electron interactions on the excitonic properties and charge-density modulations in AB-stacked double-layer (DL) graphene, placed in an external gate potential V. The coexistence of canted antiferromagnetic order and an excitonic pairing gap has been studied with the help of the generalized Hubbard model. We calculate the chemical potential μ, the average charge-density difference between the layers $\delta\bar{n}$, the antiferromagnetic gap function Δ_{AFM}, and the excitonic order parameters Δ_σ in the zero-temperature limit. We found that the excitonic pairing order parameter has a larger energy scale than the canted antiferromagnetic gap function. Charge neutrality in the DL graphene system occurs only in the absence of an external gate potential V. Moreover, we have shown that the values of the antiferromagnetic gap function Δ_{AFM} and excitonic order parameter Δ_σ are always increasing at large values of the interlayer Coulomb interaction, while they are decreasing for large values of the applied gate potential V.

DOI: 10.1103/PhysRevB.108.075147

I. INTRODUCTION

Double-layer (DL) and bilayer graphene (BLG) structures have been the subject of intensive research for a long time [1–6] due to their extraordinary physical [7–10] and mechanical properties [11]. Particularly, excitonic properties of the BLG structure represent another interesting domain of interest [12–17]. The principal achievement in this field was the observation of large values of the energy gap [18–20] and the control of the electronic spectrum of this system [21–30].

When an external electric field is applied to DL or BLG structures, changes occur in the carrier charge density of these materials. Those changes lead to unusual variations of the chemical potential, as a function of electron doping [31]. If the energy cost in the spectrum of single-particle excitation is large, then an energy gap appears in the electronic band structure [32]. Moreover, in some cases, the mentioned gap function appears also without an external electric field [33]. This situation takes place when considering the electron-electron interaction effects in double-layer structures [12,33] and also when considering the coexistence between excitonic and antiferromagnetic (AFM) orders [34–37]. The gap-function appearance, with or without an electric field, is related first of all to the complicated single-electron reconfiguration effects [38] in the layers of the BLG system. These effects are governed by the interlayer Coulomb interaction [39] and by the separation distance between the layers [40] in DL or BLG systems. More complicated physics is related to the case when considering the competing effects between AFM order [30,35] and excitonic effects [30,35,36]. Especially, it has been shown in Refs. [30,35] that an on-site Coulomb interaction stabilizes the AFM ordering which, furthermore, gets suppressed at large values of the bias voltage. Meanwhile, interlayer Coulomb repulsion and nonzero voltage stabilize the excitonic order. Here, the principal effect which leads to the formation of a gap function in an excitation spectrum is related to the formation and condensation of excitons, which recently have been the subject of many interesting experimental [38,41,42] and theoretical [34–37,43,44] investigations.

Beside numerous studies on the problem of coexistence of antiferromagnetism and excitonic order [34–37] in AA BLG and DL structures, there is a lack of treatments concerning double-layer AB or AB BLG. Particularly, the type of AFM order appears to be structurally different in AB DL systems, due to the canted character of the antiferromagnetism and which is due to the stacking type of the layers in this system. For this reason, canted antiferromagnetism (CAFM) and its coexistence with excitonic order in the AB DL system is worthy of investigation and will be the principal subject of the present paper. Here, we study AB-stacked DL graphene in the presence of an external gate potential. Moreover, we study the average charge-density imbalance between different layers, governed by an external gate potential and possible excitonic condensation states. In both layers, we consider different partial fillings (i.e., fractional average number of particles per site) of the atomic lattice sites. A particular case of this is accomplished when one has one particle per site in the upper layer, and no particle in the lower layer, i.e., the case of pumped electron-hole DL graphene. The effects of on-site and interlayer Coulomb interactions have been treated within the bilayer Hubbard model, and a mean-field analog theory was constructed to linearize the second-order interaction terms.

The paper is organized as follows: In Sec. II we introduce the Hamiltonian of the model. In Sec. III we obtain the Green's function matrix, and in Sec. IV we give the self-consistent equations. Furthermore, in Sec. V we discuss the results. At the end of the paper, in Sec. VI, we give a short conclusion to our paper. The Appendix is devoted to the calculation of some important coefficients, entering in the series of self-consistent equations.

*v.apinyan@intibs.pl

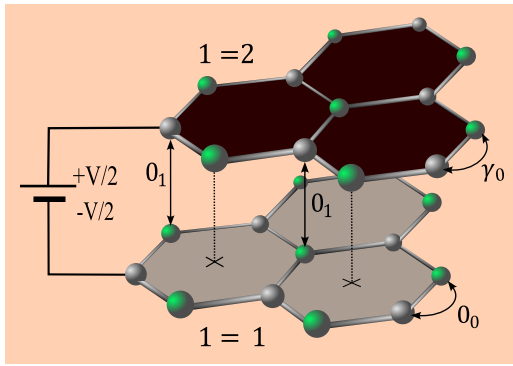

FIG. 1. The structure of AB double-layer (DL) graphene in an external electric field potential V. The layers of the system have been indicated as $\ell = 1$ (bottom layer) and $\ell = 2$ (upper layer). In the picture, the $A, \tilde{A}$ atomic sites are represented by gray balls, and the $B, \tilde{B}$ atomic sites are represented by green balls.

II. THE HAMILTONIAN OF DL GRAPHENE

Our system is described via the Hubbard Hamiltonian, written for the two layers,

$$\hat{\mathcal{H}}_{\mathrm{AB}} = \hat{\mathcal{H}}_0 + \hat{\mathcal{H}}_{\mathrm{int}} + \hat{\mathcal{H}}_{\mathrm{V}}, \tag{1}$$

where $\hat{\mathcal{H}}_0$ is the free part for the noninteracting system, $\hat{\mathcal{H}}_{\mathrm{int}}$ is the term which includes the interactions between electrons, and $\hat{\mathcal{H}}_{\mathrm{V}}$ is the Hamiltonian of coupling with an external gate potential. The free part of the Hamiltonian in Eq. (1) is

$$\begin{aligned}\hat{\mathcal{H}}_0 = &-\gamma_0 \sum_{\langle \mathbf{r}\mathbf{r}'\rangle} \sum_{\ell\sigma} [\hat{a}^\dagger_{\ell\sigma}(\mathbf{r})\hat{b}_{\ell\sigma}(\mathbf{r}') + \mathrm{H.c.}] \\ &- \gamma_0 \sum_{\langle \mathbf{r}\mathbf{r}'\rangle} \sum_{\ell\sigma} [\hat{\tilde{a}}^\dagger_{\ell\sigma}(\mathbf{r})\hat{\tilde{b}}_{\ell\sigma}(\mathbf{r}') + \mathrm{H.c.}] \\ &- \gamma_1 \sum_{\mathbf{r}\sigma} [\hat{b}^\dagger_{\sigma}(\mathbf{r})\hat{\tilde{a}}_{\sigma}(\mathbf{r}) + \mathrm{H.c.}] \\ &- \mu \sum_{\ell=1,2} \sum_{\mathbf{r}} \hat{n}_\ell(\mathbf{r}).\end{aligned} \tag{2}$$

The operators $\hat{a}_{\ell\sigma}(\mathbf{r})$, $\hat{b}_{\ell\sigma}(\mathbf{r})$, $\hat{a}^\dagger_{\ell\sigma}(\mathbf{r})$, and $\hat{b}^\dagger_{\ell\sigma}(\mathbf{r})$ in Eq. (2) are the operators of annihilation and creation for the electrons. The schematic representation of the system in consideration is shown in Fig. 1. The parameter γ_0 is the hopping amplitude of the electrons in the layers, and the energy parameter γ_1 describes the hopping of the electrons between the layers. We put for these parameters the values $\gamma_0 \sim 3$ eV and $\gamma_1 = 0.257$ eV (see Ref. [45]). The angle brackets $\langle \cdots \rangle$ in the first two terms in Eq. (2) denote the sum over nearest-neighbor lattice site positions. The index σ in Eq. (2) describes the spins of the electrons, which take two values $\sigma = \uparrow(\equiv 1), \downarrow(\equiv -1)$. Next, μ is the chemical potential in the system, coupled with the total electron density operators $\hat{n}_\ell$, for the individual layer ℓ. In turn, the operators $\hat{n}_\ell$ are defined in the following way,

$$\begin{aligned}\hat{n}_{\ell=1}(\mathbf{r}) &= \sum_\sigma \hat{a}^\dagger_\sigma(\mathbf{r})\hat{a}_\sigma(\mathbf{r}) + \hat{b}^\dagger_\sigma(\mathbf{r})b_\sigma(\mathbf{r}), \\ \hat{n}_{\ell=2}(\mathbf{r}) &= \sum_\sigma \hat{\tilde{a}}^\dagger_\sigma(\mathbf{r})\hat{\tilde{a}}_\sigma(\mathbf{r}) + \hat{\tilde{b}}^\dagger_\sigma(\mathbf{r})\hat{\tilde{b}}_\sigma(\mathbf{r}).\end{aligned} \tag{3}$$

The term $\hat{\mathcal{H}}_{\mathrm{int}}$ of the Hamiltonian in Eq. (1) describes the electron-electron interactions in the system,

$$\begin{aligned}\hat{\mathcal{H}}_{\mathrm{int}} = &U \sum_{\mathbf{r}} \sum_{\ell} \hat{n}_{\ell\uparrow}(\mathbf{r})\hat{n}_{\ell\eta\downarrow}(\mathbf{r}) \\ &+ W \sum_{\mathbf{r}} \sum_{\sigma\sigma'} \hat{n}_{b\sigma}(\mathbf{r})\hat{n}_{\tilde{a}\sigma'}(\mathbf{r}),\end{aligned} \tag{4}$$

where U is the on-site Hubbard interaction and W is the Coulomb interaction potential between the layers, which also has a local character, as the potential U. The coupling with the external electric field V is described by the Hamiltonian $\hat{\mathcal{H}}_{\mathrm{V}}$,

$$\hat{\mathcal{H}}_{\mathrm{V}} = \frac{V}{2} \sum_{\mathbf{r}} [\hat{n}_2(\mathbf{r}) - \hat{n}_1(\mathbf{r})]. \tag{5}$$

We suppose that the potential of the electric field at the upper layer (with the layer index $\ell = 2$) is $+\frac{V}{2}$ and the potential of the electric field at the bottom layer (with the layer index $\ell = 1$) is $-\frac{V}{2}$. This is represented in Fig. 1.

III. HARTREE-FOCK DECOUPLING AND ORDER PARAMETERS

To proceed, we pass to the Grassmann representation for the fermions [where the operators $\hat{a}_{\ell\sigma}(\mathbf{r})$, $\hat{b}_{\ell\sigma}(\mathbf{r})$, $\hat{a}^\dagger_{\ell\sigma}(\mathbf{r})$, and $\hat{b}^\dagger_{\ell\sigma}(\mathbf{r})$ are replaced by the complex numbers $a_{\ell\sigma}(\mathbf{r})$, $b_{\ell\sigma}(\mathbf{r})$, $\bar{a}_{\ell\sigma}(\mathbf{r})$, and $\bar{b}_{\ell\sigma}(\mathbf{r})$] and we linearize the biquadratic density terms using the Hubbard-Stratanovich transformation. The total action of the AB DL graphene system could be written as

$$\mathcal{S} = \sum_\eta \mathcal{S}_B[\bar{\eta}, \eta] + \int_0^\beta d\tau \hat{\mathcal{H}}_{\mathrm{AB}}(\tau), \tag{6}$$

where $S_B[\bar{\eta}, \eta]$ in the first term in Eq. (6) is the Berry action, which is defined as

$$\mathcal{S}_B[\bar{\eta}, \eta] = \sum_{\mathbf{r}\sigma} \int_0^\beta d\tau \bar{\eta}_\sigma(\mathbf{r}\tau)\partial_\tau \eta_\sigma(\mathbf{r}\tau), \tag{7}$$

and the summation index η indicates the type of particles, i.e.,

$$\eta = \begin{cases} a, b & \text{if } \ell = 1, \\ \tilde{a}, \tilde{b} & \text{if } \ell = 2. \end{cases} \tag{8}$$

Next, $\beta = 1/k_B T$, where T is the temperature, and the integration variable τ is the imaginary time τ, given from the interval $0 \leqslant \tau \leqslant \beta$.

Furthermore, we use the fermionic path-integral approach, already employed in Ref. [30]. The linearization procedure for the bilinear fermionic density terms is quite involved [30], and for this reason we give here only the form of the resulting action. Hubbard-Stratanovich decoupling for density-density terms in the Hamiltonian in Eq. (4) results in Hartree-Fock-like expressions for the excitonic gap parameter Δ_σ and antiferromagnetic gap function Δ_{AFM}. In particular, the antiferromagnetic gap function Δ_{AFM} for the η-type sublattice

site is

$$\Delta^{\eta}_{\rm AFM} = \frac{U}{2}\langle n_{\eta\uparrow} - n_{\eta\downarrow}\rangle. \tag{9}$$

Assuming staggered CAFM order in the system, we can write

$$\begin{aligned}
\Delta^{a}_{\rm AFM} &= -\Delta_{\rm AFM},\\
\Delta^{\tilde{a}}_{\rm AFM} &= -\Delta_{\rm AFM},\\
\Delta^{b}_{\rm AFM} &= \Delta_{\rm AFM},\\
\Delta^{\tilde{b}}_{\rm AFM} &= \Delta_{\rm AFM}.
\end{aligned} \tag{10}$$

We assume in general that $|\Delta^{\tilde{a}}_{\rm AFM}| = |\Delta^{b}_{\rm AFM}|$, because the corresponding electron densities are localized in the layers on the same lattice site positions in the x-y plane. The case when $\Delta^{\tilde{a}}_{\rm AFM} \neq \Delta^{b}_{\rm AFM}$ (representing the case of inhomogeneous CAFM order) is out of the scope of discussion in this paper. Thus, we have the following averages,

$$\begin{aligned}
\Delta_{\rm AFM} &= \frac{U}{2}\langle n_{b\uparrow} - n_{b\downarrow}\rangle,\\
\Delta_{\sigma} &= W\langle \bar{b}_{\sigma}(\mathbf{r}\tau)\tilde{a}_{\sigma}(\mathbf{r}\tau)\rangle.
\end{aligned} \tag{11}$$

The averages $\langle\cdots\rangle$ in Eq. (11) can be expressed with the help of the partition function of the system,

$$\langle\cdots\rangle = \frac{1}{Z}\int [\mathcal{D}\bar{\psi}\mathcal{D}\psi]\cdots e^{-\mathcal{S}[\bar{\psi},\psi]}, \tag{12}$$

where Z is the partition function of the AB DL system,

$$Z = \int [\mathcal{D}\bar{\psi}\mathcal{D}\psi] e^{-\mathcal{S}[\bar{\psi},\psi]}. \tag{13}$$

We have introduced in Eqs. (12) and (13) the Nambu spinors $\bar{\psi}_{\sigma}(\mathbf{k}\nu_n)$ and their conjugates fields $[\bar{\psi}_{\sigma}(\mathbf{k}\nu_n)]^T$ as

$$[\bar{\psi}_{\sigma}(\mathbf{k}\nu_n)]^T = [\bar{a}_{\sigma}(\mathbf{k}\nu_n), \bar{b}_{\sigma}(\mathbf{k}\nu_n), \bar{\tilde{a}}_{\sigma}(\mathbf{k}\nu_n), \bar{\tilde{b}}_{\sigma}(\mathbf{k}\nu_n)], \tag{14}$$

where ν_n are Matsubara frequencies for the fermionic Grassmann field $\nu_n = \pi(2n+1)/\beta$, with $n = 0, \pm1, \pm2, \ldots$. The action in Eq. (13) is represented in the following form,

$$\mathcal{S}[\bar{\psi},\psi] = \frac{1}{\beta N}\sum_{\mathbf{k}\nu_n\sigma} \bar{\psi}_{\sigma}(\mathbf{k}\nu_n)\hat{\mathcal{G}}^{-1}_{\sigma}(\mathbf{k}\nu_n)\psi_{\sigma}(\mathbf{k}\nu_n), \tag{15}$$

where $\hat{\mathcal{G}}^{-1}_{\sigma}(\mathbf{k}\nu_n)$ is the inverse Green's function matrix,

$$\hat{\mathcal{G}}^{-1}_{\sigma}(\mathbf{k}\nu_n) = \begin{pmatrix} -\mu_{1\sigma} - i\nu_n & -\tilde{\gamma}_{1\mathbf{k}} & 0 & 0\\ -\tilde{\gamma}_{2\mathbf{k}} & -\mu_{2\sigma} - i\nu_n & -\gamma_1 - \bar{\Delta}_{\sigma} & 0\\ 0 & -\gamma_1 - \Delta_{\sigma} & -\mu_{3\sigma} - i\nu_n & -\tilde{\gamma}_{2\mathbf{k}}\\ 0 & 0 & -\tilde{\gamma}_{1\mathbf{k}} & -\mu_{4\sigma} - i\nu_n \end{pmatrix}. \tag{16}$$

Here, we have introduced the effective chemical potentials μ_i with $i = 1, \ldots, 4$, for different spin directions,

$$\begin{aligned}
\mu_{i\sigma} &= \mu + (-1)^i\sigma\Delta_{\rm AFM} + \frac{V}{2} - \frac{U}{2}\bar{n}_b\\
&\quad + (-1)^{i+1}(i-1)2\sigma W,\\
\mu_{j\sigma} &= \mu + (-1)^i\sigma\Delta_{\rm AFM} - \frac{V}{2} - \frac{U}{2}\bar{n}_{\tilde{a}},
\end{aligned} \tag{17}$$

where $i = 1, 2$ and $j = 3, 4$. The chemical potentials in Eq. (17) express the effective single-particle excitation spectrum in our system, composed of four sublattices. They contain the Coulomb interactions U, W, the external gate potential V, and the CAFM order parameter $\Delta_{\rm AFM}$. The parameters $\tilde{\gamma}_{i\mathbf{k}}$ with $i = 1, 2$ in Eq. (16) are the dispersion relations in the layers of the AB DL graphene,

$$\begin{aligned}
\tilde{\gamma}_{1\mathbf{k}} &= \tilde{\gamma}_0[e^{-ik_x} + 2e^{i\frac{k_x}{2}}\cos(k_y\sqrt{3})],\\
\tilde{\gamma}_{2\mathbf{k}} &= \tilde{\gamma}_0[e^{ik_x} + 2e^{-i\frac{k_x}{2}}\cos(k_y\sqrt{3})].
\end{aligned} \tag{18}$$

We realize that $\tilde{\gamma}_{2\mathbf{k}} = \tilde{\gamma}^{*}_{1\mathbf{k}}$. In the next section, we derive the explicit form of the set of self-consistent equations.

IV. THE SELF-CONSISTENT EQUATIONS

Next, we use the partition function in Eq. (13) to calculate the average charge densities $\bar{n}_b$ and $\bar{n}_{\tilde{a}}$ at the sublattice sites B and $\tilde{A}$,

$$\begin{aligned}
\bar{n}_b &= \sum_{\sigma}\langle \bar{b}_{\sigma}(\mathbf{r}\tau)b_{\sigma}(\mathbf{r}\tau)\rangle,\\
\bar{n}_{\tilde{a}} &= \sum_{\sigma}\langle \bar{\tilde{a}}_{\sigma}(\mathbf{r}\tau)\tilde{a}_{\sigma}(\mathbf{r}\tau)\rangle.
\end{aligned} \tag{19}$$

Now, we will define the equations which describe the average particle-filling numbers (with the coefficient $1/\kappa$) and the average particle-density difference (which we note by $\delta\bar{n}$) between the layers. Those average number of particles concern the sublattices B (in the bottom layer $\ell = 1$) and $\tilde{A}$ (in the upper layer $\ell = 2$). Those equations are

$$\begin{aligned}
\bar{n}_b + \bar{n}_{\tilde{a}} &= \frac{1}{\kappa},\\
\bar{n}_{\tilde{a}} - \bar{n}_b &= \frac{\delta\bar{n}}{2}.
\end{aligned} \tag{20}$$

Then, we can calculate the averages $\bar{n}_b$ and $\bar{n}_{\tilde{a}}$ with the help of κ and $\delta\bar{n}$,

$$\begin{aligned}
\bar{n}_b &= \frac{1}{2}\left(\frac{1}{\kappa} - \frac{\delta\bar{n}}{2}\right),\\
\bar{n}_{\tilde{a}} &= \frac{1}{2}\left(\frac{1}{\kappa} + \frac{\delta\bar{n}}{2}\right).
\end{aligned} \tag{21}$$

We evaluate the statistical averages in Eqs. (11) and (19) by using the inverse Green's function matrix, given in Eq. (16). Furthermore, we combine the definitions in Eq. (11) with

those in Eq. (20) to obtain the complete set of self-consistent equations. We use also the fact that $\bar{n}_a = \bar{n}_b$ and $\bar{n}_{\tilde{a}} = \bar{n}_{\tilde{b}}$. The system of self-consistent equations for the AB DL system reads

$$\frac{1}{\kappa} = -\frac{1}{N}\sum_{i\mathbf{k},\sigma} \alpha_{i\mathbf{k}\sigma} n_F(\mu - \varepsilon_{i\sigma}(\mathbf{k})),$$

$$\frac{\delta\bar{n}}{2} = -\frac{1}{N}\sum_{i\mathbf{k},\sigma} \beta_{i\mathbf{k}\sigma} n_F(\mu - \varepsilon_{i\sigma}(\mathbf{k})),$$

$$\Delta_{\mathrm{AFM}} = -\frac{U}{2N}\sum_{i\mathbf{k},\sigma} \sigma\gamma_{i\mathbf{k}\sigma} n_F(\mu - \varepsilon_{i\sigma}(\mathbf{k})),$$

$$\Delta_\sigma = \frac{W}{N}\sum_{i\mathbf{k}} \delta_{i\mathbf{k}\sigma} n_F(\mu - \varepsilon_{i\sigma}(\mathbf{k})). \tag{22}$$

The explicit forms of the coefficients $\alpha_{i\mathbf{k}\sigma}$, $\beta_{i\mathbf{k}\sigma}$, $\gamma_{i\mathbf{k}\sigma}$, and $\delta_{i\mathbf{k}\sigma}$ in Eq. (22) are given in the Appendix. Next, the function $n_F(x)$ in Eq. (22) is the Fermi-Dirac distribution

$$n_F(x) = \frac{1}{e^{\beta(x-\mu)}+1}. \tag{23}$$

Furthermore, the energy parameters $\varepsilon_{i\sigma}(\mathbf{k})$ in Eq. (22) define the energy band structure in the AB DL graphene. They are given as

$$\varepsilon_{i\sigma}(\mathbf{k}) = \bar{\mu}_{1\sigma} + \frac{(-1)^i}{2}\sqrt{A_{\mathbf{k}\sigma} - 2\sqrt{B_{\mathbf{k}\sigma}}},$$

$$\varepsilon_{j\sigma}(\mathbf{k}) = \bar{\mu}_{2\sigma} + \frac{(-1)^j}{2}\sqrt{A_{\mathbf{k}\sigma} + 2\sqrt{B_{\mathbf{k}\sigma}}}, \tag{24}$$

where $i = 1, 2$ and $j = 3, 4$, and

$$\bar{\mu}_{1\sigma} = (\mu_{1\sigma} + \mu_{2\sigma})/2,$$

$$\bar{\mu}_{2\sigma} = (\mu_{3\sigma} + \mu_{4\sigma})/2. \tag{25}$$

The energy- and spin-dependent parameters $A_{\mathbf{k}\sigma}$ and $B_{\mathbf{k}\sigma}$ in Eq. (24) have been obtained as

$$\begin{aligned} A_{\mathbf{k}\sigma} &= 2|\Delta_\sigma + \gamma_1|^2 + 4|\tilde{\gamma}_{\mathbf{k}}|^2 + 4|\Delta_{\mathrm{AFM}}|^2 + (\mu_{1\sigma} - \mu_{2\sigma})^2, \\ B_{\mathbf{k}\sigma} &= |\Delta_\sigma + \gamma_1|^4 + 4|\Delta_\sigma + \gamma_1|^2|\tilde{\gamma}_{\mathbf{k}}|^2 \\ &\quad + 4(\mu_{1\sigma} - \mu_{2\sigma})|\Delta_\sigma + \gamma_1|^2\Delta_{\mathrm{AFM}} \\ &\quad + 4(\mu_{1\sigma} - \mu_{2\sigma})^2(|\tilde{\gamma}_{\mathbf{k}}|^2 + |\Delta_{\mathrm{AFM}}|^2). \end{aligned} \tag{26}$$

In the following, we solve numerically the system of equations (22) with the help of Newton's fast convergent algorithm. We will discuss the obtained results in the next section.

V. RESULTS

Here, we will discuss the main results obtained in the present paper. In Fig. 2, we calculate numerically the chemical potential μ and the excitonic order parameter $\Delta_\uparrow$. In Fig. 2(a), the chemical potential is presented as a function of the interlayer Coulomb interaction potential W. Several values of the on-site Coulomb potential U [see Eq. (4)] have been considered in the picture. Different average particle-filling regimes have been used. All results have been done in the zero-temperature limit $T = 0$, and the external gate potential was set at a value $V = \gamma_0$. The black (red) curves show the

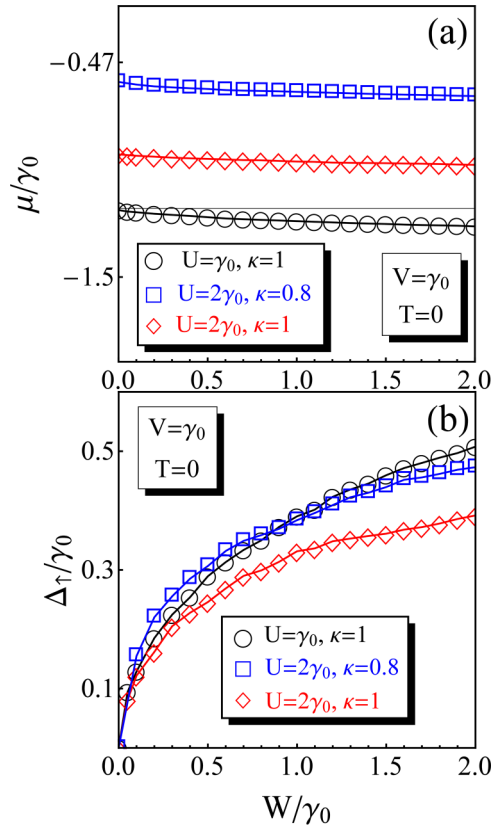

FIG. 2. The numerical results for (a) μ and (b) $\Delta_\uparrow$, as a function of the interlayer Coulomb interaction parameter W. The calculations have been done in the zero-temperature limit, and different values of the interaction parameter U and inverse-filling coefficient κ have been considered. The external gate potential has been fixed at a value $V = \gamma_0 = 3$ eV.

$\mu(W)$ dependence for $U = \gamma_0$ ($U = 2\gamma_0$), and correspond to the case $\kappa = 1$. The blue-squared points correspond to the case of the smaller value of the coefficient κ, namely $\kappa = 0.8$. The value $\kappa = 1$ corresponds to the case when the AB DL was initially pumped with the electrons in the upper layer and the holes in the lower layer, or vice versa. We see that μ is nearly constant as a function of W. The negative values of μ indicate the possibility of the existence of a stable excitonic condensate state [33]. The same nearly constant behavior was observed for the average charge-density imbalance function $\delta\bar{n}$ [see Fig. 3(b)]. We observe also that the values of the obtained chemical potential are smaller (with modulus) for the smaller value of the coefficient κ, namely for $\kappa = 0.8$ [see the blue curve in Fig. 2(a)]. This means that the energy cost for the creation of the single-particle excitation is lower in that case. We see in Fig. 3(b) that the values of the function $\delta\bar{n}$ are negative for all considered values of the potential U. This fact shows that the system is in the regime of the hole-electron DL, i.e., there are fewer electrons in the upper layer than in the bottom layer ($\bar{n}_2 < \bar{n}_1$). The calculated excitonic order parameter $\Delta_\uparrow$ and the CAFM gap function Δ_{AFM} have been showed respectively in Figs. 2(b) and 3(a). We see that they both are monotonically increasing functions of W, i.e., they are continuously increasing with W, for all values of the localizing Coulomb potential U. In addition, we see that the

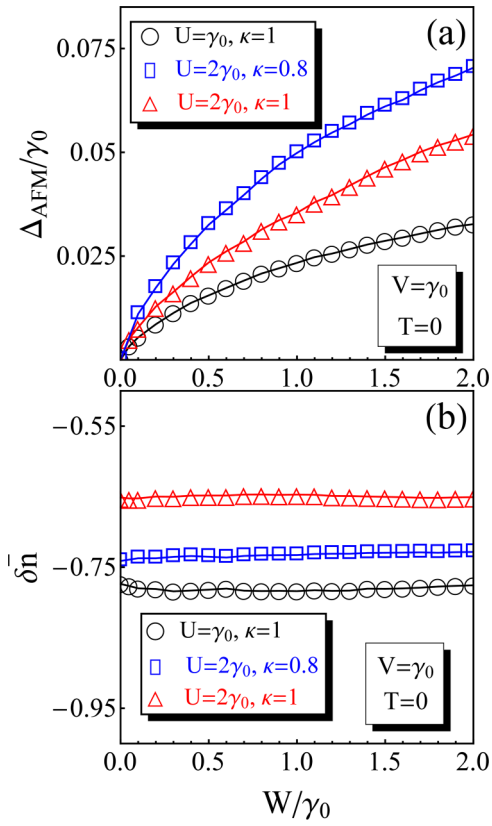

FIG. 3. The numerical results for (a) Δ_{AFM} and (b) $\delta\bar{n}$, as a function of the interlayer Coulomb interaction parameter W. The calculations have been done in the zero-temperature limit, and different values of the interaction parameter U and inverse-filling coefficient κ have been considered. The external gate potential has been fixed at a value $V = \gamma_0 = 3$ eV.

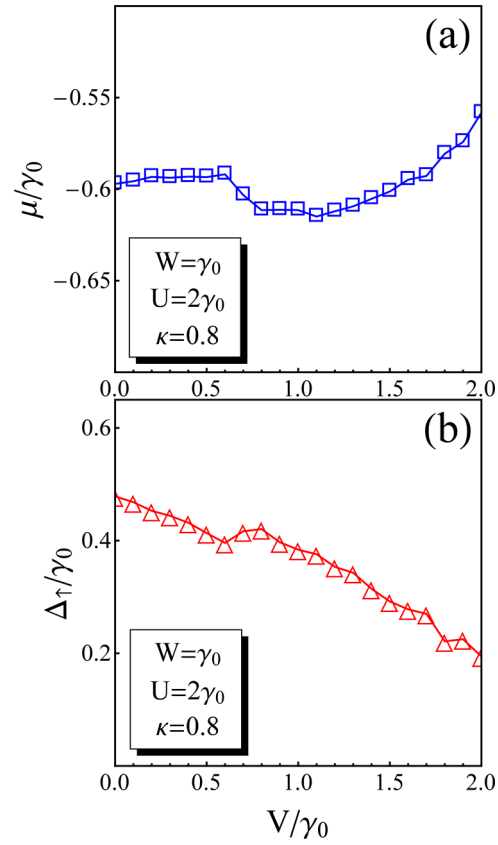

FIG. 4. The numerical results for (a) μ and (b) $\Delta_{\uparrow}$, as a function of the gate potential V. The calculations have been done in the zero-temperature limit $T = 0$. The Coulomb interaction parameter U, the interlayer interaction W, and the inverse-filling coefficient κ have been set respectively at the values $U = 2\gamma_0$, $W = \gamma_0$, and $\kappa = 0.8$.

excitonic and CAFM order parameters get larger values in the case of the small value of the inverse-filling coefficient κ, notably for $\kappa = 0.8$. This is directly related to the fact that the chemical potential μ takes small values in that case [see blue-square points in Fig. 2(a)], i.e., when the energy cost for single-particle excitations in the system is lower.

Furthermore, in Figs. 4 and 5 we have shown the V dependence of the same physical quantities. The results in Figs. 4 and 5 have been done for the case $W = \gamma_0$, $U = 2\gamma_0$, and $\kappa = 0.8$. The calculations were performed in the zero-temperature limit. We see in Fig. 4(a) that $\mu < 0$ for all considered values of the applied gate potential V. The excitonic order parameter and the CAFM deviation function are no longer open functions [see Figs. 4(b) and 5(a)]. Particularly, they are decreasing when one increases the gate potential parameter V, from zero up to the value $V = 2\gamma_0$. The general strategy for finding the dependence on V for the excitonic gap function is to fix the distance between the layers, which therefore will lead to the fixed numerical value for the interlayer Coulomb interaction W and for the Hubbard-U local interaction. Those values have been show in Figs. 4 and 5. Namely, we have $W = \gamma_0 = 3$ eV and $U = 2\gamma_0 = 6$ eV. The average charge-density imbalance $\delta\bar{n}$ shown in Fig. 5(b) decreases dramatically with V, being always negative, i.e., $\delta\bar{n}(V) < 0$ ($\bar{n}_2 < \bar{n}_1$). Moreover, for large values of V (see the values of V in $\gamma_0 \leqslant V \leqslant 2\gamma_0$), the average charge imbalance between the layers becomes very large and the layer with $\ell = 2$ becomes depopulated from electrons. Thus, by increasing the external potential we reconfigure the electron distributions in the layers and the upper layer with $\ell = 2$ becomes pumped from the electrons. We observe also that the exact charge neutrality ($\delta\bar{n} = 0$) occurs only at the value $V = 0$ of the external gate potential.

VI. DISCUSSIONS AND CONCLUSION

We have studied the coexistence of excitonic and antiferromagnetic orders in double-layer AB-stacked graphene. The external gate voltage was applied to the DL structure. Principal attention has been paid to the Coulomb interaction effects in the bilayer system, which have been treated with the help of the bilayer Hubbard Hamiltonian. In addition, the electronic energy spectrum was obtained using effective chemical potentials. Partial filling has been considered in this paper, i.e., when the average number of electrons at a given lattice site position is less than one.

The numerical calculations have been performed by using Newton's fast convergent algorithm, and the results have been obtained at the zero-temperature limit. The calculated negative values of the chemical potential in the system show the possibility of the existence of an excitonic condensate state in

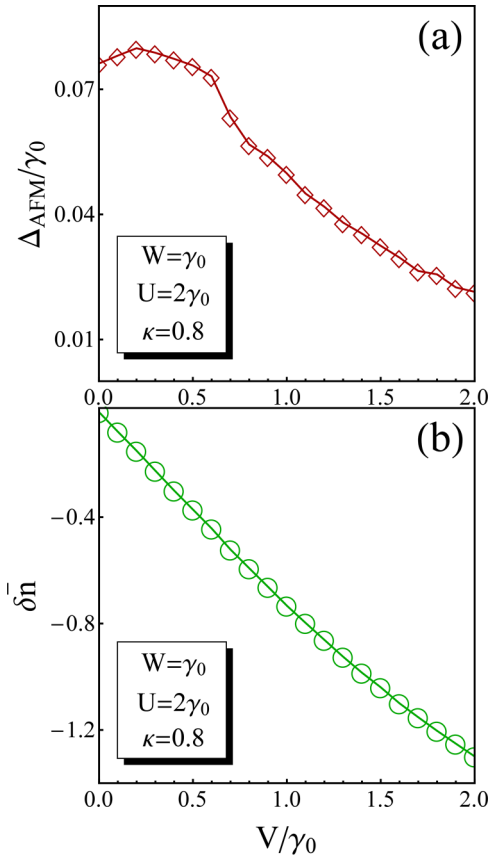

FIG. 5. The numerical results for (a) Δ_{AFM} and (b) $\delta\bar{n}$, as a function of the gate potential V. The calculations have been done in the zero-temperature limit $T = 0$. The Coulomb interaction parameter U, the interlayer interaction W, and the inverse-filling coefficient κ have been set respectively at the values $U = 2\gamma_0$, $W = \gamma_0$, and $\kappa = 0.8$.

the DL system, which can be tuned by varying the separation distance between the layers in the DL structure. We have shown that the energy scales of the excitonic order parameter $\Delta_\uparrow$ are much larger than the energy scales corresponding to the CAFM gap, i.e., $\Delta_\uparrow \gg \Delta_{\mathrm{AFM}}$. This finding is just the opposite of the result in Ref. [30], where it has been shown that the AFM gap is much larger than the excitonic order parameter, i.e., $\Delta_{\mathrm{AFM}} \gg \Delta_\uparrow$. Moreover, the excitonic order parameter survives only for one spin direction, particularly for $\sigma = \uparrow$.

Another interesting observation is that the average charge imbalance $\delta\bar{n}$ is always negative for all values of the Coulomb interaction between the layers and of the electric field potential which are given in the intervals $0 \leqslant W \leqslant 2\gamma_0$ and $0 \leqslant V \leqslant 2\gamma_0$. Therefore, the average number of electrons in the upper layer is always less than in the lower layer. The AB DL system, with this type of configuration, could be interesting for modern technological applications [45–49] and is more useful owing to the high speed of electrons in the graphene layers [50–52]. The changes in the charge imbalance with the applied gate potential show the possibility of tuning the AB DL system from an electron-electron to an electron-hole type when increasing the external gate potential V. The exact charge neutrality, i.e., when $\delta\bar{n} = 0$, occurs only at the zero value of the external voltage $V = 0$. The charge imbalance is stronger for large values of V, which means that large values of V effectively stabilize the electron-hole-type bilayer rather than the electron-electron one. For fixed V, the variation of $\delta\bar{n}$, as a function of W, is almost constant, so it appears that the average charge imbalance is indifferent to changes in the distance of separation between layers. Moreover, all nonzero values of the gate potential have a destructive effect on the excitonic gap parameter, while the antiferromagnetic gap function increases at relatively small values of V, especially when $0 \leqslant V \leqslant 0.2\gamma_0$.

To summarize, the chemical potential and the charge-density imbalance between the layers are constant linear functions of the Coulomb potential between the layers and therefore they do not depend on the charge modulations in the layers and the separation distance between layers. The excitonic and CAFM order parameters are increasing functions of the interaction parameter. The applied gate potential changes the physical parameters more significantly than the Coulomb interaction between the layers (note that the Coulomb potential between the layers varies when changing the separation distance between the layers). We have shown that the energy scales, corresponding to the CAFM order parameter, are much smaller than the excitonic energy scales and we attribute this result to the stacking type of the system, i.e., AB stacking of the layers. It is worth noting that in the case of AA-type stacked DL graphene, the result is exactly the opposite [30] and an opposite effect occurs for the mentioned energy scales.

We think that the results obtained in the paper could be important from both theoretical and experimental points of view. In particular, the energy scales of the antiferromagnetic and excitonic orders were unexpectedly modified when considering the effect of CAFM in the AB-stacked double layer, instead of AA type of stacking (for comparison, see the results in Ref. [30]). The results in this paper could be helpful also for applications of the AB DL system in modern electronics, optoelectronics, and photonics technologies as a device where the electron density reconfigurations and optical properties are simultaneous changed.

APPENDIX: THE CALCULATION OF IMPORTANT COEFFICIENTS

In this Appendix, we show the explicit forms of the coefficients, the parameters entering in the right-hand sides of Eqs. (22). Particularly, we have

$$\alpha_{i\mathbf{k}\sigma} = \begin{cases} \frac{(-1)^{i+1}}{\varepsilon_{1\sigma}(\mathbf{k})-\varepsilon_{2\sigma}(\mathbf{k})} \prod_{j=3,4} \frac{\mathcal{P}^{(3)}[\varepsilon_{i\sigma}(\mathbf{k})]}{[\varepsilon_{i\sigma}(\mathbf{k})-\varepsilon_{j\sigma}(\mathbf{k})]}, & \text{if } i = 1, 2, \\ \frac{(-1)^{i+1}}{\varepsilon_{3\sigma}(\mathbf{k})-\varepsilon_{4\sigma}(\mathbf{k})} \prod_{j=1,2} \frac{\mathcal{P}^{(3)}[\varepsilon_{i\sigma}(\mathbf{k})]}{[\varepsilon_{i\sigma}(\mathbf{k})-\varepsilon_{j\sigma}(\mathbf{k})]}, & \text{if } i = 3, 4, \end{cases} \tag{A1}$$

where the band-structure quasienergies $\varepsilon_{i\sigma}(\mathbf{k})$ (with $i = 1, \ldots, 4$) have been obtained at the end of Sec. IV and the third-order polynomial $\mathcal{P}^{(3)}(x)$ in Eq. (A1) is defined as

$$\mathcal{P}^{(3)}(x) = 2x^3 + a_{1\sigma}x^2 + b_{1\sigma}x + c_{1\sigma}. \tag{A2}$$

Here,

$$\begin{aligned} a_{1\sigma} &= -3(\bar{\mu}_{1\sigma} + \bar{\mu}_{2\sigma}), \\ b_{1\sigma} &= -2|\tilde{\gamma}_{\mathbf{k}}|^2 - 2\Delta_{\mathrm{AFM}}^2 + 2\sigma(\bar{\mu}_{1\sigma} - \bar{\mu}_{2\sigma})\Delta_{\mathrm{AFM}} \\ &\quad + (\bar{\mu}_{1\sigma} + \bar{\mu}_{2\sigma})^2 + 2\bar{\mu}_{1\sigma}\bar{\mu}_{2\sigma}, \\ c_{1\sigma} &= (\bar{\mu}_{1\sigma} + \bar{\mu}_{2\sigma})|\tilde{\gamma}_{\mathbf{k}}|^2 + (\bar{\mu}_{1\sigma} + \bar{\mu}_{2\sigma})\Delta_{\mathrm{AFM}}^2 \\ &\quad + \sigma\left(\bar{\mu}_{2\sigma}^2 - \bar{\mu}_{1\sigma}^2\right) - \bar{\mu}_{1\sigma}\bar{\mu}_{2\sigma}(\bar{\mu}_{1\sigma} + \bar{\mu}_{2\sigma}). \end{aligned} \tag{A3}$$

Next, in the second of equations in the system (22), we get for the coefficient $\beta_{i\mathbf{k}\sigma}$,

$$\beta_{i\mathbf{k}\sigma} = \begin{cases} \frac{(-1)^{i+1}}{\varepsilon_{1\sigma}(\mathbf{k}) - \varepsilon_{2\sigma}(\mathbf{k})} \prod_{j=3,4} \frac{\mathcal{P}^{(2)}[\varepsilon_{i\sigma}(\mathbf{k})]}{[\varepsilon_{i\sigma}(\mathbf{k}) - \varepsilon_{j\sigma}(\mathbf{k})]}, & \text{if } i = 1, 2, \\ \frac{(-1)^{i+1}}{\varepsilon_{3\sigma}(\mathbf{k}) - \varepsilon_{4\sigma}(\mathbf{k})} \prod_{j=1,2} \frac{\mathcal{P}^{(2)}[\varepsilon_{i\sigma}(\mathbf{k})]}{[\varepsilon_{i\sigma}(\mathbf{k}) - \varepsilon_{j\sigma}(\mathbf{k})]}, & \text{if } i = 3, 4, \end{cases} \tag{A4}$$

with $\mathcal{P}^{(2)}(x)$ defined as

$$\mathcal{P}^{(2)}(x) = a_{2\sigma}x^2 + b_{2\sigma}x + c_{2\sigma}, \tag{A5}$$

where

$$\begin{aligned} a_{2\sigma} &= -2\sigma\Delta_{\mathrm{AFM}} - \bar{\mu}_{1\sigma} + \bar{\mu}_{2\sigma}, \\ b_{2\sigma} &= 2\sigma(\bar{\mu}_{1\sigma} + \bar{\mu}_{2\sigma})\Delta_{\mathrm{AFM}} + \bar{\mu}_{1\sigma}^2 - \bar{\mu}_{2\sigma}^2, \\ c_{2\sigma} &= 2\Delta_{\mathrm{AFM}}^3 - (\bar{\mu}_{1\sigma} - \bar{\mu}_{2\sigma})|\tilde{\gamma}_{\mathbf{k}}|^2 - (\bar{\mu}_{1\sigma} - \bar{\mu}_{2\sigma})\Delta_{\mathrm{AFM}}^2 \\ &\quad - \bar{\mu}_{1\sigma}\bar{\mu}_{2\sigma}(\bar{\mu}_{1\sigma} - \bar{\mu}_{2\sigma}) - \left(\bar{\mu}_{1\sigma}^2 + \bar{\mu}_{2\sigma}^2\right)\Delta_{\mathrm{AFM}} \\ &\quad + 2|\tilde{\gamma}_{\mathbf{k}}|^2\Delta_{\mathrm{AFM}}. \end{aligned} \tag{A6}$$

Furthermore, we get for the coefficient $\gamma_{i\mathbf{k}\sigma}$ in the third equation in Eq. (22),

$$\gamma_{i\mathbf{k}\sigma} = \begin{cases} \frac{(-1)^{i+1}}{\varepsilon_{1\sigma}(\mathbf{k}) - \varepsilon_{2\sigma}(\mathbf{k})} \prod_{j=3,4} \frac{\mathcal{P}'^{(2)}[\varepsilon_{i\sigma}(\mathbf{k})]}{[\varepsilon_{i\sigma}(\mathbf{k}) - \varepsilon_{j\sigma}(\mathbf{k})]}, & \text{if } i = 1, 2, \\ \frac{(-1)^{i+1}}{\varepsilon_{3\sigma}(\mathbf{k}) - \varepsilon_{4\sigma}(\mathbf{k})} \prod_{j=1,2} \frac{\mathcal{P}'^{(2)}[\varepsilon_{i\sigma}(\mathbf{k})]}{[\varepsilon_{i\sigma}(\mathbf{k}) - \varepsilon_{j\sigma}(\mathbf{k})]}, & \text{if } i = 3, 4, \end{cases} \tag{A7}$$

where $\mathcal{P}'^{(2)}(x)$ is

$$\mathcal{P}'^{(2)}(x) = a_{3\sigma}x^2 + b_{3\sigma}x + c_{3\sigma}, \tag{A8}$$

with

$$\begin{aligned} a_{3\sigma} &= 2\Delta_{\mathrm{AFM}}, \\ b_{3\sigma} &= 4\mu_2\Delta_{\mathrm{AFM}}, \\ c_{3\sigma} &= 2\mu_2^2\Delta_{\mathrm{AFM}} - 2\Delta_{\mathrm{AFM}}^3 - 2|\tilde{\gamma}_{\mathbf{k}}|^2\Delta_{\mathrm{AFM}}. \end{aligned} \tag{A9}$$

The coefficient $\delta_{\mathbf{k}\sigma}$ in the last equation in Eq. (22) was obtained as

$$\delta_{i\mathbf{k}\sigma} = \begin{cases} \frac{(-1)^{i+1}}{\varepsilon_{1\sigma}(\mathbf{k}) - \varepsilon_{2\sigma}(\mathbf{k})} \prod_{j=3,4} \frac{\mathcal{P}_{\Delta}^{(2)}[\varepsilon_{i\sigma}(\mathbf{k})]}{[\varepsilon_{i\sigma}(\mathbf{k}) - \varepsilon_{j\sigma}(\mathbf{k})]}, & \text{if } i = 1, 2, \\ \frac{(-1)^{i+1}}{\varepsilon_{3\sigma}(\mathbf{k}) - \varepsilon_{4\sigma}(\mathbf{k})} \prod_{j=1,2} \frac{\mathcal{P}_{\Delta}^{(2)}[\varepsilon_{i\sigma}(\mathbf{k})]}{[\varepsilon_{i\sigma}(\mathbf{k}) - \varepsilon_{j\sigma}(\mathbf{k})]}, & \text{if } i = 3, 4, \end{cases} \tag{A10}$$

where

$$\begin{aligned} \mathcal{P}_{\Delta}^{(2)}(x) &= -(\Delta_{\sigma} + \gamma_1)[x^2 - x(\bar{\mu}_{1\sigma} + \bar{\mu}_{2\sigma}) - \Delta_{\mathrm{AFM}}^2 \\ &\quad + \sigma(\bar{\mu}_{1\sigma} - \bar{\mu}_{2\sigma})\Delta_{\mathrm{AFM}} + \bar{\mu}_{1\sigma}\bar{\mu}_{2\sigma}]. \end{aligned} \tag{A11}$$

Let us mention at the end that the coefficients $\alpha_{i\mathbf{k}\sigma}$ in Eq. (A1) are dimensionless due to the structure of the polynomials $\mathcal{P}^{(3)}(x)$ given in Eq. (A2), while the coefficients $\beta_{i\mathbf{k}\sigma}$, $\gamma_{i\mathbf{k}\sigma}$, and $\delta_{i\mathbf{k}\sigma}$ in Eqs. (A4), (A7), and (A10) have a dimension of the inverse energy.

[1] K. Yan, H. Peng, Y. Zhou, H. Li, and Zh. Liu, Formation of bilayer Bernal graphene: Layer-by-layer epitaxy via chemical vapor deposition, Nano Lett. **11**1106 (2011).

[2] S. Jin, J. Zong, W. Chen, Q. Tian, X. Qiu, G. Liu, H. Zheng, X. Xi, L. Gao, C. Wang, and Y. Zhang, Epitaxial growth of uniform single-layer and bilayer graphene with assistance of nitrogen plasma, Nanomaterials **11**, 3217 (2021).

[3] Z. Yan, P. Zhiwei, S. Zhengzong, Y. Jun, Y. Zhu, Zh. Liu, P. M. Ajayan, and J. M. Tour, Growth of bilayer graphene on insulating substrates, ACS Nano **5**, 8187 (2011).

[4] H. Wang, Z. Yao, G. S. Jung, Q. Song, M. Hempel, T. Palacios, G. Chen, M. J. Buehler, A. Aspuru-Guzik, and J. Kong, Frank-van der Merwe growth in bilayer graphene, Matter **5**, 3339 (2021).

[5] F. Wenjing, H. Allen and L. Song, and K. Jing, A review of large-area bilayer graphene synthesis by chemical vapor deposition, Nanoscale **7**, 20335 (2015).

[6] N. R. Abdullah, H. O. Rashid, C.-S. Tang, A. Manolescu, and V. Gudmundsson, Controlling physical properties of bilayer graphene by stacking orientation caused by interaction between B and N dopant atoms, Mater. Sci. Eng., B **276**, 115554 (2022).

[7] E. McCann and M. Koshino, The electronic properties of bilayer graphene, Rep. Prog. Phys. **5**, 056503 (2013).

[8] C. Park, J. Ryou, S. Hong, B. G. Sumpter, G. Kim, and M. Yoon, Electronic Properties of Bilayer Graphene Strongly Coupled to Interlayer Stacking and an External Electric Field, Phys. Rev. Lett. **115**, 015502 (2015).

[9] X. Yao, X. Zhang, X. Yeb, and J. Wang, Structure and electronic properties of bilayer graphene functionalized with half-sandwiched transition metal-cyclopentadienyl complexes, Phys. Chem. Chem. Phys. **18**, 22390 (2016).

[10] Y. Y. Zhang, C. M. Wang, Y. Cheng, and Y. Xiang, Mechanical properties of bilayer graphene sheets coupled by sp^3 bonding, Carbon **49**, 4511 (2011).

[11] V. Apinyan and T. K. Kopeć, Excitonic condensation and metal-semiconductor transition in AA bilayer graphene in an external magnetic field, Phys. Rev. B **105**, 184503 (2022).

[12] V. Apinyan and T. K. Kopeć, Spectral properties of excitons in the bilayer graphene, Physica E **95**, 108 (2018).

[13] M. Ohm Sauer and Th. G. Pedersen, Exciton absorption, band structure, and optical emission in biased bilayer graphene, Phys. Rev. B **105**, 115416 (2022).

[14] L. Yang, J. Deslippe, Ch.-H. Park, M. L. Cohen, and S. G. Louie, Excitonic Effects on the Optical Response of Graphene and Bilayer Graphene, Phys. Rev. Lett. **103**, 186802 (2009).
[15] T.-H.-H. Do, D.-T. Bui, and V.-N. Phan, Excitonic properties in a double-layer graphene, Phys. Scr. **97**, 105707 (2022).
[16] L. Ju, L. Wang, T. Cao, T. Taniguchi, K. Watanabe, S. G. Louie, F. Rana, J. Park, J. Hone, F. Wang, and P. L. McEuen, Tunable excitons in bilayer graphene, Science **358**, 907 (2017).
[17] C. H. Lui, Zh. Li, K. F. Mak, E. Cappelluti, and T. F. Heinz, Observation of an electrically tunable band gap in trilayer graphene, Nat. Phys **7**, 944 (2011).
[18] K. F. Mak, Ch. H. Lui, J. Shan, and T. F. Heinz, Observation of an Electric-Field-Induced Band Gap in Bilayer Graphene by Infrared Spectroscopy, Phys. Rev. Lett. **102**, 256405 (2009).
[19] Y. Liu, W. S. Lew, and Z. Liu, Observation of anomalous resistance behavior in bilayer graphene, Nanoscale Res. Lett. **12**, 48 (2017).
[20] E. Icking, L. Banszerus, W. Frederike, F. Volmer, P. Schmidt, C. Steiner, S. Engels, J. Hesselmann, M. Goldsche, K. Watanabe, T. Taniguchi, C. Volk, B. Beschoten, and C. Stampfer, Transport spectroscopy of ultraclean tunable band gaps in bilayer graphene, Adv. Electron. Mater. **8**, 2200510 (2022).
[21] M. Alattas and U. Schwingenschlögl, Band gap control in bilayer graphene by co-doping with B-N pairs, Sci. Rep. **8**, 17689 (2018).
[22] S. M. Choi, S. H. Jhi, and Y. W. Son, Controlling energy gap of bilayer graphene by strain, Nano Lett. **10**, 3486 (2010).
[23] Y. Zhang, C. H. Hu, Y. H. Wen, S. Q. Wu, and Z. Z. Zhu, Strain-tunable band gap of hydrogenated bilayer graphene, New J. Phys. **13**, 063047 (2011).
[24] Z. Peng, X. Chen, Y. Fan, D. J. Srolovitz, and D. Lei, Strain engineering of 2D semiconductors and graphene: From strain fields to band-structure tuning and photonic applications, Light: Sci. Appl. **9**, 190 (2020).
[25] A. O. Sboychakov, A. V. Rozhkov, A. L. Rakhmanov, and F. Nori, Externally Controlled Magnetism and Band Gap in Twisted Bilayer Graphene, Phys. Rev. Lett. **120**, 266402 (2018).
[26] G. O. Abdullaev and Z. Z. Alisultanov, Electronic spectrum of bilayer graphene with broken P-symmetry of both intra- and inter-layers, Physica E **123**, 114192 (2020).
[27] B. L. Huang, C. P. Chuu, and M. F. Lin, Asymmetry-enriched electronic and optical properties of bilayer graphene, Sci. Rep. **9**, 859 (2019).
[28] A. S. Mayorov, D. C. Elias, M. Mucha-Kruczynski, R. V. Gorbachev, T. Tudorovskiy, A. Zhukov, S. V. Morozov, M. I. Katsnelson, A. K. Geim, and K. S. Novoselov, Interaction-driven spectrum reconstruction in bilayer graphene, Science **333**, 860 (2011).
[29] A. O. Sboychakov, A. L. Rakhmanov, A. V. Rozhkov, and F. Nori, Electronic spectrum of twisted bilayer graphene, Phys. Rev. B **92**, 075402 (2015).
[30] V. Apinyan and T. K. Kopeć, Antiferromagnetic ordering and excitonic pairing in AA-stacked bilayer graphene, Phys. Rev. B **104**, 075426 (2021).
[31] K. Lee, B. Fallahazad, J. Xue, D. C. Dillen, K. Kim, T. Taniguchi, K. Watanabe, and E. Tutuc, Chemical potential and quantum Hall ferromagnetism in bilayer graphene, Science **345**, 58 (2014).
[32] S. Kim, I. Jo, D. C. Dillen, D. A. Ferrer, B. Fallahazad, Z. Yao, S. K. Banerjee, and E. Tutuc, Direct Measurement of the Fermi Energy in Graphene Using a Double-Layer Heterostructure, Phys. Rev. Lett. **108**, 116404 (2012).
[33] V. Apinyan and T. K. Kopeć, Excitonic gap formation and condensation in the bilayer graphene structure, Phys. Scr. **91**, 095801 (2016).
[34] R. S. Akzyanov, A. O. Sboychakov, A. V. Rozhkov, A. L. Rakhmanov, and F. Nori, AA-stacked bilayer graphene in an applied electric field: Tunable antiferromagnetism and coexisting exciton order parameter, Phys. Rev. B **90**, 155415 (2014).
[35] A. O. Sboychakov, A. V. Rozhkov, A. L. Rakhmanov, and F. Nori, Antiferromagnetic states and phase separation in doped AA-stacked graphene bilayers, Phys. Rev. B **88**, 045409 (2013).
[36] A. L. Rakhmanov, A. V. Rozhkov, A. O. Sboychakov, and F. Nori, Instabilities of the *AA*-Stacked Graphene Bilayer, Phys. Rev. Lett. **109**, 206801 (2012).
[37] A. L. Rakhmanov, A. V. Rozhkov, A. O. Sboychakov, and F. Nori, Phase separation of antiferromagnetic ground states in systems with imperfect nesting, Phys. Rev. B **87**, 075128 (2013).
[38] R. N. Wang, G. Y. Dong, S. F. Wang, G. S. Fu, and J. L. Wang, Intra- and inter-layer charge redistribution in biased bilayer graphene, AIP Adv. **6**, 035213 (2016).
[39] V. N. Phan and H. Fehske, Coulomb interaction effects in graphene bilayers: Electron-hole pairing and plasmaron formation, New J. Phys. **14**, 075007 (2012).
[40] A. Sinner and K. Ziegler, Effect of the Coulomb interaction on the gap in monolayer and bilayer graphene, Phys. Rev. B **82**, 165453 (2010).
[41] B. Fallahazad, K. Lee, S. Kang, J. Xue, S. Larentis, C. Corbet, K. Kim, H. Movva, T. Taniguchi, K. Watanabe, L. F. Register, S. K. Banerjee, and E. Tutuc, Gate-tunable resonant tunneling in double bilayer graphene heterostructures, Nano Lett. **15**, 428 (2014).
[42] J. I. A. Li, T. Taniguchi, K. Watanabe, J. Hone, and C. R. Dean, Excitonic superfluid phase in double bilayer graphene, Nat. Phys. **13**, 751 (2017).
[43] L. Yang, Excitons in intrinsic and bilayer graphene, Phys. Rev. B **83**, 085405 (2011).
[44] P. Li and I. Appelbaum, Excitons without effective mass: Biased bilayer graphene, Phys. Rev. B **99**, 035429 (2019).
[45] M. Mucha-Kruczyński, E. McCann, and V. I. Fal'ko, Electron-hole asymmetry and energy gaps in bilayer graphene, Semicond. Sci. Technol. **25**, 033001 (2010).
[46] J. Tian, A. Katsounaros, D. Smith, and Y. Hao, Graphene field-effect transistor model with improved carrier mobility analysis, IEEE Transactions on Electron Devices **62**, 3433 (2015).
[47] F. Pasadas and D. Jiménez, Large-signal model of the bilayer graphene field-effect transistor targeting radio-frequency applications: Theory versus experiment, J. Appl. Phys. **118**, 244501 (2015).
[48] M. Tian, Q. Hu, C. Gu, X. Xiong, Z. Zhang, X. Li, and Y. Wu, Tunable $1/f$ Noise in CVD Bernal-stacked bilayer graphene transistors, ACS Appl. Mater. Interfaces **12**, 17686 (2020).

[49] Y. Sabir, A. Shams, M. Sabir, and M. Ahmed, Modeling of bilayer graphene based field effect transistors for digital electronics, Int. J. Innov. Sci. Res. **10**, 262 (2014).

[50] K. S. Bhargavi and S. S. Kubakaddi, High field transport properties of a bilayer graphene, Physica E **56**, 123 (2014).

[51] X. Li, K. M. Borysenko, N. M. Buongiorno, and K. W. Kim, Electron transport properties of bilayer graphene, Phys. Rev. B **84**, 195453 (2011).

[52] L. F. Sun, L. M. Dong, Z. F. Wu, and C. Fang, A comparison of the transport properties of bilayer graphene, monolayer graphene, and two-dimensional electron gas, Chin. Phys. B **22**, 077201 (2013).